

Focused-electron-beam-induced processing (FEBIP) for emerging applications in carbon nanoelectronics

Andrei G. Fedorov · Songkil Kim · Mathias Henry ·
Dhaval Kulkarni · Vladimir V. Tsukruk

Received: 24 February 2014 / Accepted: 14 July 2014 / Published online: 27 July 2014
© Springer-Verlag Berlin Heidelberg 2014

Abstract Focused-electron-beam-induced processing (FEBIP), a resist-free additive nanomanufacturing technique, is an actively researched method for “direct-write” processing of a wide range of structural and functional nanomaterials, with high degree of spatial and time-domain control. This article attempts to critically assess the FEBIP capabilities and unique value proposition in the context of processing of electronics materials, with a particular emphasis on emerging carbon (i.e., based on graphene and carbon nanotubes) devices and interconnect structures. One of the major hurdles in advancing the carbon-based electronic materials and device fabrication is a disjoint nature of various processing steps involved in making a functional device from the precursor graphene/CNT materials. Not only this multi-step sequence severely limits the throughput and increases the cost, but also dramatically reduces the processing reproducibility and negatively impacts the quality because of possible between-the-step contamination, especially for impurity-susceptible materials such as graphene. The FEBIP provides a unique opportunity to address many challenges of carbon nanoelectronics, especially when it is employed as part of an integrated processing environment based on multiple “beams” of

energetic particles, including electrons, photons, and molecules. This avenue is promising from the applications’ prospective, as such a multi-functional (electron/photon/molecule beam) enables one to define shapes (patterning), form structures (deposition/etching), and modify (cleaning/doping/annealing) properties with locally resolved control on nanoscale using the same tool without ever changing the processing environment. It thus will have a direct positive impact on enhancing functionality, improving quality and reducing fabrication costs for electronic devices, based on both conventional CMOS and emerging carbon (CNT/graphene) materials.

1 Introduction

As the feature sizes of electronic devices decrease to nanoscale, copper resistivity increases due to electron scattering at the surface and grain boundaries and wire-type structures become more vulnerable to electromigration damage [1–3]. As alternative materials, carbon nanoelectronics has emerged based on carbon nanotubes (CNTs) and graphene, which are being actively explored owing to their unique electronic transport characteristics, as well as their excellent mechanical and thermal properties [3–8]. Despite an intriguing potential of graphene/CNT-based materials and structures for nanoelectronic devices, a number of fundamental limitations still provide significant roadblocks to application of these materials to real device platforms [3]. Among them, the most significant challenge is a large electrical contact resistance between CNTs/graphene and metal terminals. Recently, significant progress has been made in assessing the contact resistance of metal contacts to single-walled CNTs (SWCNTs) [9, 10]. It was found that contact resistance to a metallic SWCNT can

A. G. Fedorov (✉) · S. Kim · M. Henry
George W. Woodruff School of Mechanical Engineering,
Georgia Institute of Technology, Atlanta, GA 30332, USA
e-mail: AGF@gatech.edu

A. G. Fedorov
Parker H. Petit Institute for Bioengineering and Bioscience,
Georgia Institute of Technology, Atlanta, GA 30332, USA

D. Kulkarni · V. V. Tsukruk
School of Materials Science and Engineering, Georgia Institute
of Technology, Atlanta, GA 30332, USA

be reduced down to the quantum limit (~ 6.5 k Ω) with the channel length scaled down to 15 nm [9]. One of compelling applications is to utilize a multi-walled CNT (MWCNT) as an interconnect link and to make connection to multiple conducting shells, acting as parallel conducting channels. However, it is challenging to connect multiple conducting shells of a MWCNT using standard metal deposition processes due to the limited control of directionality (in three dimensions) in a standard contact fabrication process using nanolithography followed by metal evaporation/sputtering [11, 12].

Theoretical calculations revealed that physical contact resistance between metal and an open end of a carbon nanotube is on the order of 3–4 k Ω even for contamination-free interface [8, 13]. Also, metal deposition using sputtering or evaporation only yields a physical contact (i.e., via weak van der Waals interactions) to the MWCNT, which results in an inefficient electronic coupling at the Fermi surface [14, 15]. Thus, alternative fabrication methods have been demonstrated for establishing chemical binding of multiple CNT shells to metal [11, 12, 16]. For example, a TEM-AFM combination with the piezomotor-driven nanomanipulator was utilized to precisely position an open end of a MWCNT in contact with a tungsten AFM tip; then, the MWCNT and the tip were fused by Joule heating to establish a multiple shell contact to the metal. Such a composite MWCNT-carbide-metal interface resulted in a very low contact resistance of 700 Ω [16]. Obviously, while yielding a high-quality electrical contact, this technique is not amenable for the scalable fabrication of electronic devices and the contact area/geometry between a MWCNT and a metal tip is limited to whatever spontaneously forms in the course of an intense heat release at the contact junction with rather poor control over the final outcome.

For graphene, the contact resistance challenges are similar to that of CNTs. Physical contacts of metal to graphene by conventional metal deposition methods resulted in the contact resistivity of $2e-4$ Ω -m with Au/Pd/Ti metal contacts [17]. In order to improve contact resistance, double contacts (both at the top and bottom surface) of metal to graphene were suggested, and 40 % reduction of contact resistance was achieved compared to a single metal contact to graphene [18]. However, it still resulted in a contact resistivity of an order of $1e-4$ Ω -m, which is much higher than graphene's channel electrical resistivity. Theoretically, based on the density functional theory (DFT) calculations, the primary contribution to the contact resistance is the nature of the electronic coupling relying on the binding properties of the interface [19, 20]. Simulations suggest that the "end-contact" geometry should result in a significantly lower contact resistance than the "side-contact" geometry since the dangling bonds at the edges of

MWCNT/graphene will form the covalent bonds to metal resulting in strong electronic coupling between MWCNT/graphene and metal electrodes. For example, Ti "end-contact" interface has 10 times higher binding energy and also 10 times lower contact resistance than the "side-contact" interface between the same materials. However, the end contact is difficult to achieve experimentally using conventional metal deposition methods due to the limited control of directionality and presence of hydrogen-terminated edges of graphene, impeding chemical binding to metal. The current state of the art is on the order of 10^{-4} Ω -m lowest electrical contact resistivity demonstrated with conventional fabrication methods using Ti contact, which is still an order of magnitude higher than that of the theoretically predicted optimal end contact between graphene and metal and also for silicon-metal contacts in the CMOS device structures [19–21]. Therefore, alternative techniques are still needed to reduce contact resistivity without any side-effects of the contact fabrication process on devices.

Focused-electron-beam-induced deposition (FEBID) of graphitized carbon interface at the CNTs/graphene-metal junction has unique potential to resolve the above-mentioned challenges. The FEBID, a resist-free "direct-write" additive nanomanufacturing technique, is an emerging chemical vapor deposition (CVD) method for deposition of a variety of materials with high degree of spatial and time-domain control, [22] with pattern resolution of ~ 2 –3 nm [23] and down to sub-nanometer scale for atomically thin suspended substrates [24]. Of particular interest to CNT/graphene electronics is deposition of carbon using secondary electron mediated dissociation of surface-adsorbed hydrocarbon precursors. [25, 26] Due to formation of highly reactive hydrocarbon radical intermediates during deposition procedure, there are reasons to expect that FEBID carbon will form strong chemical binding to MWCNT/graphene [27, 28]. Also, deposition of the contact material can be precisely controlled in FEBID (both the rate of growth and the resulting 3D shape of the contact interface) by changing the electron beam current and accelerating voltage [25, 29, 30] and moving the electron beam relative to the deposition substrate. A fundamental challenge with any beam-based fabrication methods is limited scalability to making contacts simultaneously to many devices in parallel. FEBID is no exception in this regard, but recent advances in developing a multi-beam FEBID system provide a pathway for at least partially mitigating the scale-up challenge [31].

An overarching goal of this opinion article is to critically assess the FEBIP capabilities and its unique value proposition in the context of processing of electronics materials, with particular emphasis on emerging carbon (CNT and graphene) devices and interconnect structures. As such it is not intended to be a comprehensive review of

the state of the art, but rather our reflection through a lens of recently demonstrated capabilities and achievements by our group aiming to identify the opportunities for major advances and to stimulate further research in the field of FEBIP for nanoelectronics. To this end, we first introduce our long-term vision of multi-functional FEBIP environment for “direct-write” manufacturing of electronic materials using a synergetic combination of electron, photon, and molecular beams. Second, we summarize our achievements of the past decade in realizing different aspects of this vision, including development of FEBIP fabrication protocols for reducing the intrinsic contact resistance through chemical bonding by FEBID graphitic carbon nanostructures at the MWCNT-metal and graphene-metal interfaces. Third, we discuss opportunities for using FEBIP for direct-write patterning/etching of graphene, as well as the utility of energetic inert gas jets for impurity/doping management of the conduction channel of graphene-based devices. Lastly, we briefly present a hybrid FEBIP-MaCE (Metal-assisted Chemical Etching) technique for manufacturing 3D complex, high-aspect-ratio nanostructures useful for optoelectronic and metamaterials applications. We conclude the article with a brief summary of key lessons learned and outlook for the future.

2 FEBIP promise and opportunities

In his famed speech “There’s plenty of room at the bottom” in 1959, Richard Feynman outlined a vision of future for focused beam enabled additive nanomanufacturing—“The next question is: How do we write it? We have no standard technique to do this now. But let me argue that it is not as difficult as it first appears to be. We can reverse the lenses of the electron microscope in order to demagnify as well as magnify. A source of ions, sent through the microscope lenses in reverse, could be focused to a very small spot. We could write with that spot like we write in a TV cathode ray oscilloscope, by going across in lines, and having an adjustment which determines the amount of material which is going to be deposited as we scan in lines.” This visionary prediction by one of the greatest physicists of the twentieth century is in essence the foundational premise for FEBIP, which has been transformed to reality in the last 20+ years and is now maturing to the level of having an increasing impact on important practical applications. Nanoelectronics is one such application and is the focus of discussion in this article.

Generally speaking, focused electron (FEBIP) and ion (FIBIP) beam deposition/etching are complimentary nanoscale direct-write processing techniques, as both rely on secondary electrons generated upon interactions of the primary beam electrons and ions, respectively, to facilitate

desired deposition or dissociation (etching) chemistry of surface-bound precursor molecules. However, despite higher deposition/etching rate and greater purity of FIBIP deposits, for nanoelectronics application the use of FEBIP is preferred. This is not only due to greater resolution of electron-beam-generated nanostructures, but also, and perhaps more importantly due to significant damage and potential for parasitic chemical doping of the substrate when ion beam processing is utilized. This is especially critical for highly sensitive substrates, such as graphene, for which even slight mechanical/structural and chemical changes may result in substantial modification of electronic properties, such as bandgap, carrier mobility, and work function. Yet, it should be noted that many of the process enhancement concepts introduced next for nanoelectronics applications in conjunction with FEBIP could be readily adopted for other applications, including those for which FIBIP may be equally useful or even preferred.

2.1 Vision of multi-functional FEBIP for “direct-write” mask-less processing of electronic materials

One of the major hurdles in advancing the carbon-based electronic materials and devices (i.e., based on graphene sheets and carbon nanotubes) is a disjoint nature of various processing steps involved in making a functional device from the “raw” substrate materials. For example, it is well known that any lithographic steps in patterning graphene leave photoresist residues that affect the electronic properties of the resulting device. Or making a connection between the CNT/graphene and metal interconnects in a heterogeneous device requires multiple incompatible steps, ranging CNT dispersion and alignment, graphene ribbon cutting and/or opening the CNT ends, lithographic definition of contacts, and eventually metal evaporation to form a contact. Not only this multi-step sequence severely limits the throughput and increases the cost, but also dramatically reduces the processing reproducibility and negatively impacts the quality because of possible between-the-steps contamination, especially for impurity-susceptible materials such as graphene.

The FEBIP provides a unique opportunity to address these grand challenges of carbon nanoelectronics. A compelling long-term vision for the field is development of a forward-looking multi-functional “direct-write” nanomanufacturing process, based on focused electron/molecule/photon beams to enable a lithography-free, single-step patterning (i.e., via direct nanoscale etching/cutting), interconnection (i.e., via deposition of a bridge material forming joints between the heterogeneous devices), and doping state control (i.e., via control of adsorbed surface impurities) of the emerging carbon-based electronic materials. Importantly, the aim is to perform all of

these processes within the same processing environment (i.e., without ever leaving the processing chamber) with nanoscale resolution. This is accomplished using a combination of (1) a focused, high kinetic energy molecular gas jet (for in situ substrate cleaning from contaminant or/and dopant precursor introduction by impact dissociation/selective sticking), [32–34] (2) focused electron-beam-induced processing FEBIP (for in situ etching and joining CNT/graphene to other materials) using controlled injection of either reactive (water vapor/oxygen) or dissociative (hydrocarbons) precursors for carbon etching and deposition steps, respectively, [25, 35–38] and finally (3) nanoscale local annealing and phase transformation (e.g., carbon graphitization) of deposited nanostructures/interfaces via plasmon-enhanced absorption of photons delivered by a focused laser beam at room temperature [39–41].

2.2 FEBID carbon as interfacial material for CNT/graphene devices

Extensive investigations of CNT/graphene-metal interfaces have been performed both theoretically and experimentally in the past decade [14–21, 42]. Based on the literature review, it can be concluded that the intrinsic contact resistance depends on electronic coupling at the CNTs/graphene and metal interface, which is defined by the binding properties (i.e., physical/van der Waals vs. chemical/covalent bonding). Among possible contact metals, Ti was found to be the best candidate featuring the lowest, Ohmic contact resistance with strong binding energy of -6 kcal/mol for the “side-contact” and -80 kcal/mol for the

“end-contact” interface to graphene [14]. FEBID allows the use of a variety of materials for forming a contact junction [33]. Of particular interest to CNT and graphene electronics is carbon deposition using readily available hydrocarbon precursors. Carbon is superior as an interfacial material in that an intrinsic resistance of the contact to the CNT/graphene can be made negligibly small since carbon has good wettability to both metals (e.g., Cu) and CNT/graphene [35, 43]. Additionally, the MWCNT/graphene–carbon–metal junction should have Ohmic behavior due to similarity of work functions for all three materials involved in forming the junction [43–45].

In order to understand how FEBID carbon interacts with graphene, FEBID process of a methane molecule on graphene basal plane is modeled by sequentially removing hydrogen atom (‘dissociation’) and optimizing graphene structure with FEBID intermediate species (‘adsorption’), using density functional theory (DFT) calculation. Density functional theory (DFT) is a well-developed quantum mechanics simulation tool for atomistic understanding of molecular interactions of materials, such as binding and electronic properties [19, 20, 46]. As shown in Fig. 1, electron-beam-induced deposition of each intermediate (CH_3 , CH_2 , CH , C) establishes strong chemical binding to the basal plane (‘side-contact’) of graphene with modification of the graphene’s atomic structure. For example, FEBID of carbon on graphene yields the binding energy of -55.35 kcal/mol, which is much stronger than that of the ‘side contact’ of Ti to graphene and comparable to that of the ‘end contact’ of Ti to graphene. This result implies that FEBID carbon contact should help improve contact interface between graphene and metal electrodes.

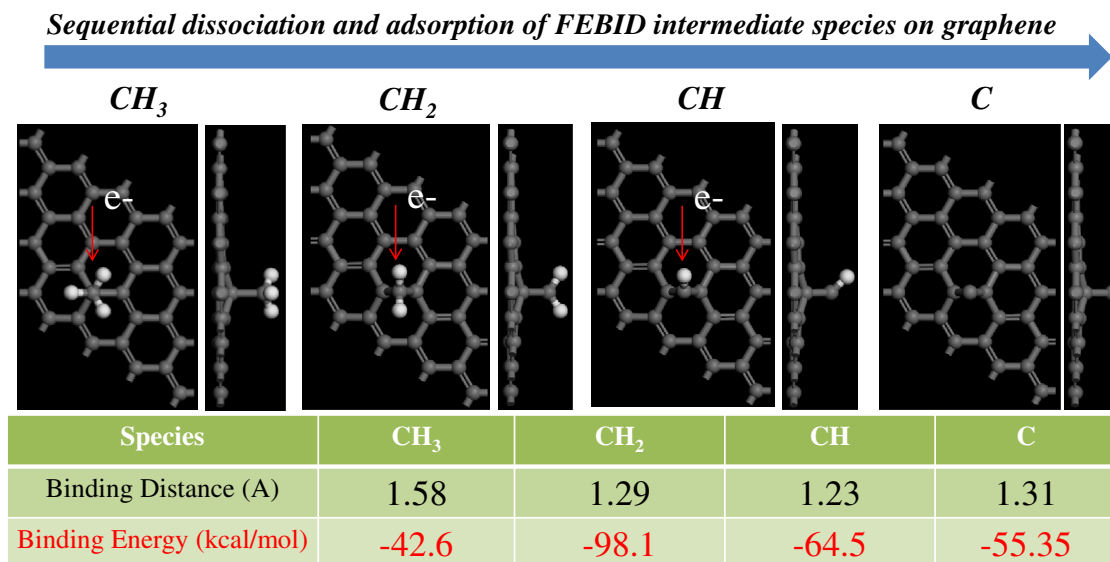


Fig. 1 DFT simulation results for electron-beam-induced sequential dissociation and adsorption of FEBID radical intermediates on the basal plane of graphene. Table *inset* shows the binding properties for each intermediate radical and graphene

2.3 Plasmon-enhanced low temperature graphitization of FEBID carbon nanostructures

Initial composition of FEBID carbon nanojoints is known to be hydrogenated amorphous structure which has high electrical resistivity of an order of $10^3 \Omega\text{-m}$ [46, 47]. Thermal annealing is therefore required to induce carbon graphitization in order to improve its electrical resistance, which has to be performed at moderate temperatures under a stringent limit of less than 400 °C as imposed by ITRS for electronics manufacturing. [3] We have developed an experimental methodology and performed a comprehensive investigation of FEBID carbon interface composition and amorphous-to-graphitic phase transitions using a combination of Raman, Atomic Force and Conductive Force Microscopies (AFM and CFM, respectively) (Figs. 2, 3). The formation of graphitic, highly conductive carbon from

initially amorphous FEBID carbon deposits can be monitored with characteristic Raman graphitic band at $1,580 \text{ cm}^{-1}$. Raman studies on the as grown FEBID amorphous carbon subjected to thermal annealing revealed that the transition from amorphous carbon to graphitic phase occurs around 250 °C and is fully completed at 350 °C, resulting in formation of nanocrystalline graphite (Fig. 2c) [35]. Moreover, specifics of this transformation further depend upon the geometry and size of the carbon deposits in form of lines and dots with characteristic dimension from 500 to 100 nm, common for carbon joints required for making connection to electronic devices. AFM measurements on these carbon deposits showed a dramatic decrease in carbon dimension which is caused by the densification of carbon deposit due to transformation from amorphous carbon phase to graphitic phase (Fig. 2a, b). In complimentary study, we observed that surface plasmons

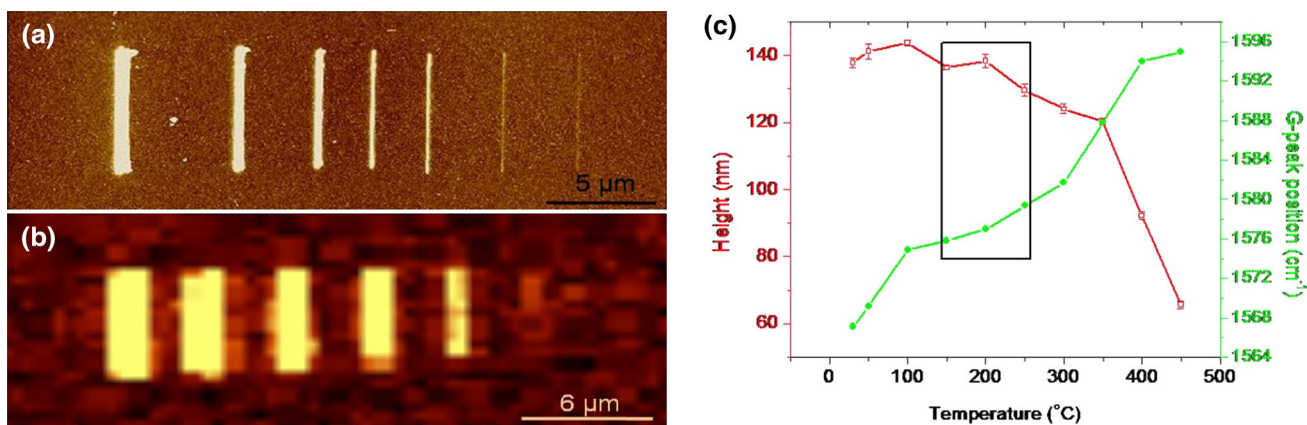


Fig. 2 **a** AFM image of FEBID carbon lines on SiO₂ substrate and **b** corresponding Raman mapping. **c** Raman G-band position and height of carbon lines showing the phase transition to fully

graphitized, nanocrystalline state within the temperature range (boxed in figure) between 150 and 250 °C

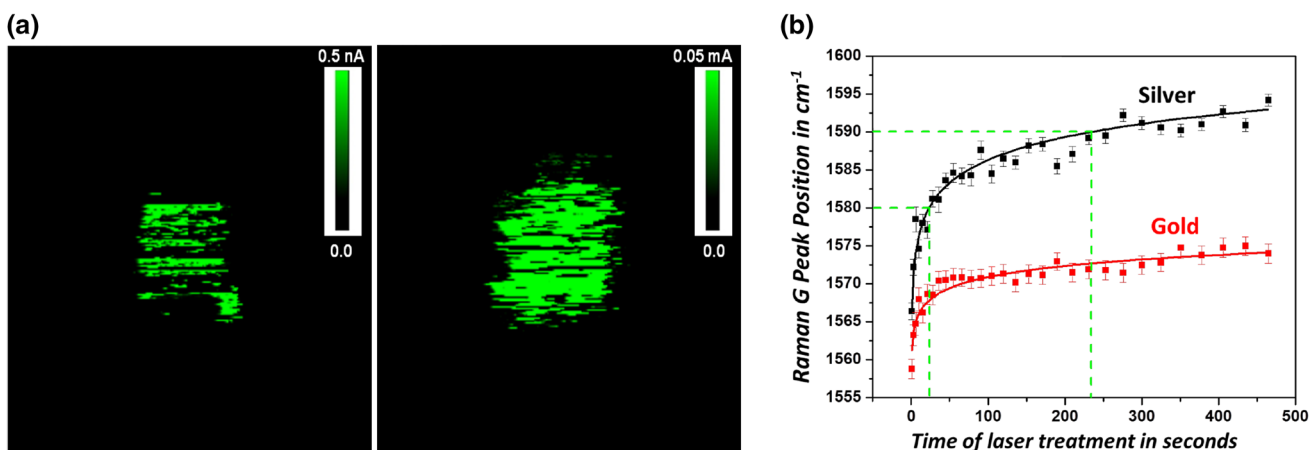


Fig. 3 **a** CFM mapping of electric current (conductivity) across the FEBID carbon film deposited on gold (left panel) and silver (right panel) substrate, indicating ~7 orders of magnitude increase (compare the current magnitude for the same applied CFM tip bias) in the carbon electrical conductivity due to plasmon-assisted

graphitization on silver substrate at room temperature. **b** Evolution of the Raman G-band position, showing faster carbon graphitization kinetics on silver as compared to the gold substrate for the laser-assisted localized annealing of FEBID carbon films

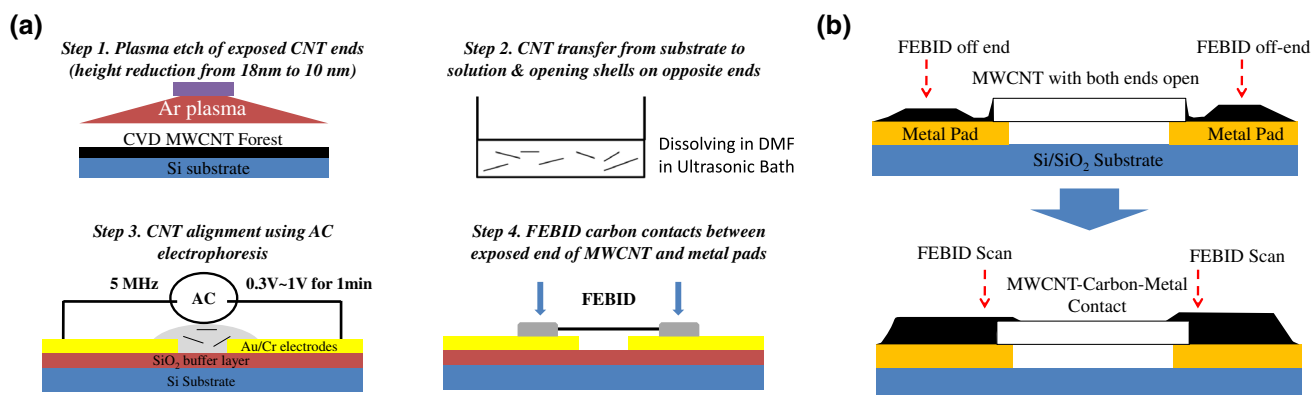


Fig. 4 Schematics of fabrication protocol of an ultra-low-resistant MWCNT-metal interconnect via FEBID graphitic nanojoints, including **a** a sequence of process steps, and **b** details of FEBID graphitic

play a key role in graphitizing the FEBID carbon deposits grown on metals (Cu, Ag, Au) surfaces and substantially improving their electrical conductivity (Fig. 3) [40]. We observed that simple scanning of the FEBID carbon grown on rough metal substrates, especially silver, under appropriate laser excitation source served as an excellent technique to locally graphitize the amorphous carbon deposits, which, importantly, occurs under the globally low (room) temperature conditions. Further, the tightly focused laser beam (514 nm) concentrated on the FEBID carbon structure only helps in avoiding any physical damage to the CNT or graphene channel, which is an important motivation for its incorporation as part of the proposed tri-functional FEBIP environment for fabrication of electronic devices.

2.4 FEBID for 3D sculpturing and modification of graphitic interfaces to CNTs and graphene

As stated in the introduction, reducing the contact resistance at the CNT/graphene-metal interfaces down to its intrinsic limit is foundational to the field of carbon nanoelectronics and therefore provides an excellent opportunity for demonstrating the FEBIP-enabled capability to address this challenging problem. Here, we discuss this topic as two interrelated themes, one is focusing on FEBID of the MWCNT-metal interface and another one is on forming contact structures to graphene devices, and describe a comprehensive framework for development of fabrication protocols and electrical/structural characterization of FEBID graphitic carbon contacts to the open-ended MWCNTs. Specifically, a complete sequence of processing steps was developed, starting from opening and exposing the multiple conducting shells of MWCNTs, following by dielectrophoretic alignment of multiple MWCNTs between metal electrodes in an array, to finally making the FEBID graphitic carbon nanostructures at the exposed ends of

nanojoint fabrication setup, resulting in connection of multiple conducting shells of MWCNT to metal terminals to form high electric performance interconnect link

MWCNTs, which successfully established an Ohmic “end” contact to multiple conducting channels of MWCNTs [35]. This resulted in demonstration of the record low contact resistance $\sim 116 \Omega$, which is an order of magnitude lower than the best results reported in literature to date. Using these advances in application of FEBID to sculpturing the graphitic carbon interfaces, three fabrication strategies of electrical contacts using graphitic nanojoints are demonstrated experimentally between the multilayered graphene and a metal interconnect [36]. This early original work is important in its own rights, but also provides a solid scientific foundation for further activities to realize the vision of multi-functional FEBIP of electronic materials.

2.4.1 FEBID of ultra-low resistance ohmic contact to MWCNTs

We have demonstrated the robust FEBID fabrication protocols for connection of multiple conducting channels of MWCNTs to metal electrodes via the FEBID graphitic nanojoints [35]. As illustrated in Fig. 4, the fabrication protocol consists of four steps. Starting with CVD grown vertically aligned MWCNT forest, one end of MWCNTs is opened using Ar plasma etching so that multiple conducting shells of MWCNTs are exposed. MWCNTs are further broken down into small pieces by releasing MWCNTs from the substrate and dispersing in dimethylformamide (DMF) by ultrasonication, thus opening the other end of MWCNT. After aligning open-ended MWCNTs onto the prefabricated interconnect using dielectrophoresis (DEP), FEBID carbon nanojoints are made using a process shown in Fig. 4b, connecting multiple conducting channels/shells of MWCNTs to the metal electrodes (Fig. 4a). Unique to this approach is that the optimal FEBID sequence was “designed” on the computer using comprehensive FEBID simulations [35, 48], which suggested the off-end electron

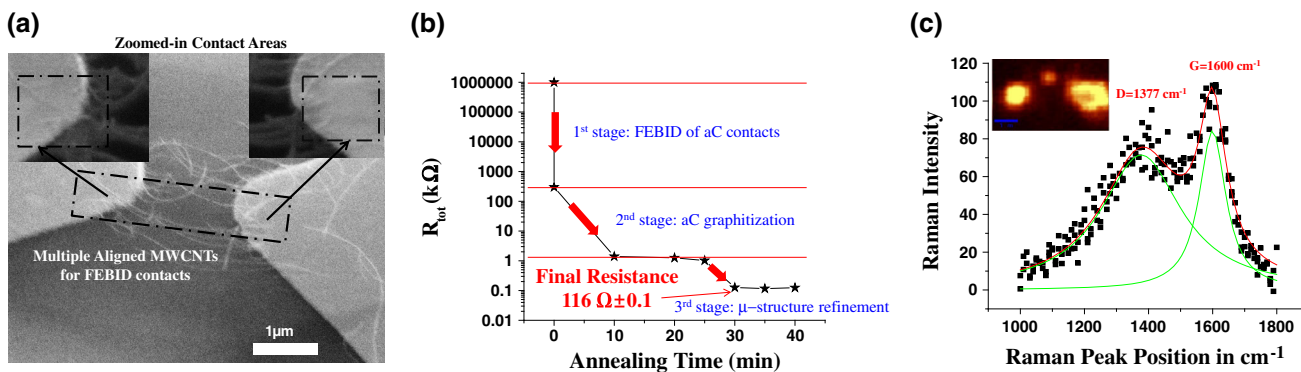


Fig. 5 **a** SEM image of MWCNT-metal interconnect with FEBID graphitic nanojoints (*insets*), **b** electrical measurements—three stages of reduction of the overall interconnect resistance with FEBID carbon nanojoint fabrication and subsequent annealing, and **c** Raman

beam positioning during deposition for forming a desired “end-contact” geometry of the contact interface with carbon film making a lateral connection to multiple CNT shells [49].

In order to graphitize the FEBID carbon nanojoints, thermal annealing was performed at 350 °C followed by two-terminal electrical measurements. Figure 5b shows the reduction of the device resistance upon increasing the annealing time for graphitization of FEBID carbon deposits. During the first stage, formation of EBID amorphous carbon nanojoints increases contact area between the MWCNT and metal electrode, leading to four order of magnitude reduction of electrical resistance from 1 GΩ to 300 kΩ. During the second stage, the FEBID amorphous carbon nanojoints are graphitized, further increasing their conductivity and connecting metal electrodes to the multiple conducting channels of MWCNT. During the third stage, additional thermal annealing improves the interfacial/electrical properties of the contact interface to MWCNT, ultimately resulting in the total interconnect resistance of $(116.0 \pm 0.1) \Omega$, which is 10^7 times smaller than without FEBID graphitic nanojoints [35]. Figure 5c shows a representative Raman spectrum of the FEBID carbon nanojoints after thermal annealing for 30 min. In Raman spectrum of carbon structures, D band corresponds to the breathing mode of sp^2 sites in rings and G-band relates to the stretching vibration of any pair of sp^2 sites in chains or aromatic rings [39, 50]. In case of amorphous carbon structures, the D-mode stretch is proportional to the probability of finding a sixfold ring in the cluster, which in turn is proportional to the cluster area. Thus, the development of the D peak indicates ordering of carbon atoms into the sp^2 -like networks [43]. Also, the D/G area ratio is known to be a quantitative factor in determining the size of graphitic crystallites in any carbon structure. It is accepted that the increase in the D/G ratio corresponds to the increase in the correlation length of the graphitic crystallites. It was shown

spectrum of FEBID graphitic nanojoints indicating the characteristics of nanocrystalline graphite with inset showing a Raman map of G peak domains (*brightest areas*) of FEBID graphitic contact interface indicating that the deposits are fully graphitized

that the D/G ratio for carbon materials varies between 0 (100 % amorphous carbon) and ~2.5 (fully nanocrystalline graphite) [39, 50]. In the measured Raman spectrum in Fig. 5c, G-band and D-band peak positions and their area ratio ($D/G = 2.55$) of the FEBID carbon nanojoints indicate the characteristics of nanocrystalline graphite whose electrical resistivity is on the order of $10^{-6} \Omega\text{-m}$ [46]. The inset of Fig. 5c shows the Raman mapping of graphitic contact structures with bright domains corresponding to the highest (graphitic) G-band peak areas.

2.4.2 FEBID graphitic nanojoints for graphene-metal contact

We have extended application of FEBID to making graphene-metal interconnects in order to reduce contact resistance at the graphene-metal interface. Three fabrication protocols for forming a multilayer (ML) graphene-metal interconnect via FEBID ‘overlayer’ (Device structure I), “post-deposited” (Device structure II) and “pre-deposited” (Device structure III) ‘interlayer’ were developed, as described in Fig. 6. ML graphene was obtained by mechanical exfoliation from highly ordered pyrolytic graphite (HOPG) using a scotch tape and transfer onto SiO_2 (90 nm)/Si substrate.

The smallest thickness of the ML graphene samples used in this work was ~3 nm, which corresponds to ~9 layers of graphene sheets. Thus, all the ML graphene samples are expected to have no response to perpendicular external electric field, which means that electrical conductivity should be constant regardless of the gate voltage (V_g) modulation [51]. Also, since the work functions (WFs) of all three contact materials are similar in range (graphene: 4.6 eV, amorphous carbon: 4.5 eV, and Cr/Au: 4.3 eV), all the devices should exhibit the Ohmic behavior [43, 44, 52]. This was confirmed by three-terminal (d: drain, s: source, g: gate) electrical measurements ($I_{ds} - V_{ds}$

Fig. 6 Schematic of the three strategies for fabrication of graphene-metal interconnects via FEBID graphitic nanojoints

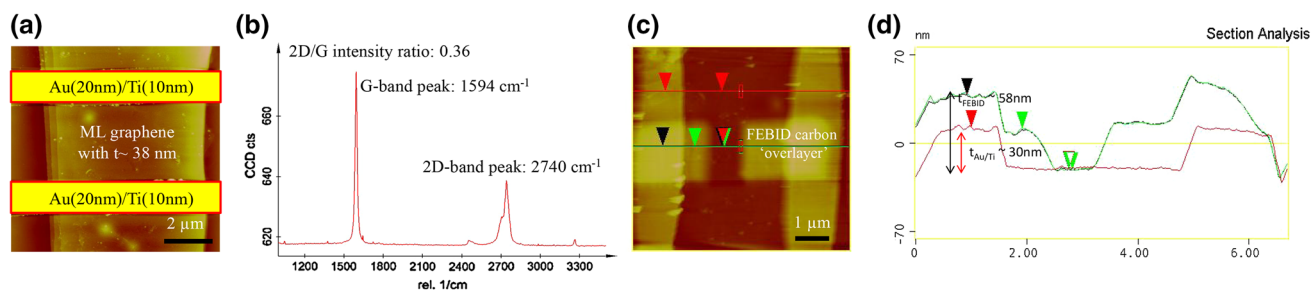
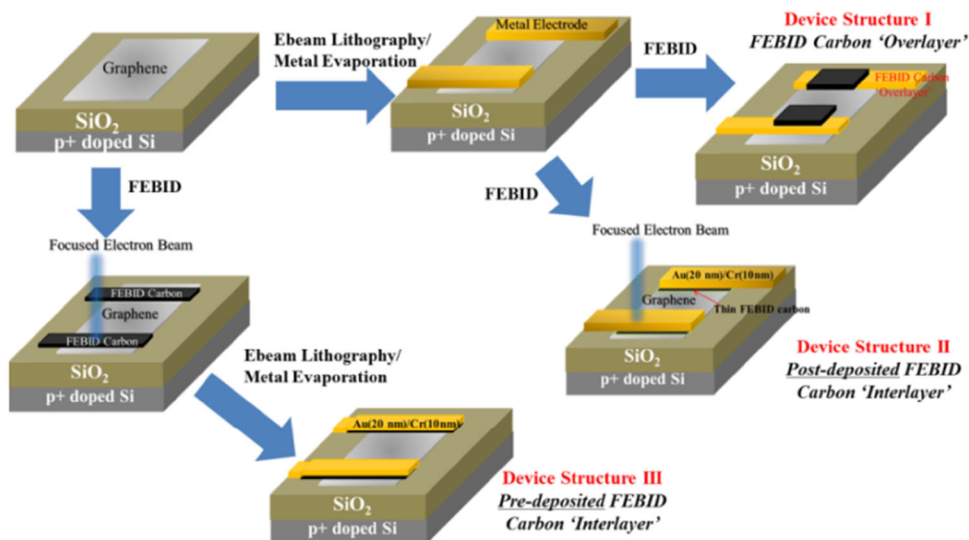


Fig. 7 **a** AFM image of the as-fabricated ML graphene-metal device, **b** Raman spectrum of ML graphene showing its high quality, **c** AFM image of a device with FEBID carbon ‘overlayers’ formed at both

electrodes and **d** AFM sectional profile showing connection of the ML graphene and metal electrodes via FEBID carbon ‘overlayers’

and $I_{ds} - V_g$) for all the device structures, and accordingly, we evaluated the device resistance from $I_{ds} - V_{ds}$ using the linear fitting based on the Ohm’s law. All electrical measurements were performed using a two-terminal method at a fixed gate voltage of $V_g = 0$ V.

Device structure I adds an additional conductive path through the FEBID carbon ‘overlayer’ nanojoints between the ML graphene and metal terminals. An interconnect between the 38-nm-thick ML graphene and metal electrodes, as shown in Fig. 7a, was fabricated using e-beam lithography followed by Au (30 nm)/Ti (10 nm) deposition using e-beam evaporator and lift-off procedure. The ML graphene was characterized using confocal Raman spectroscopy with minimum laser power. In the Raman spectrum of graphene or graphite, D-band peak is related to increase of the disorder in sp^2 sites, and thus, low D/G intensity ratio indicates high quality of graphene. Accordingly, we can conclude that the ML graphene has high quality with vanishing D/G ratio as shown in Fig. 7b, c) shows the device structure with FEBID carbon ‘overlayer’ nanojoints covering one-third of one graphene-metal contact width. The sectional

AFM profile of the device in Fig. 7d shows the thickness profile of metal electrodes and FEBID carbon ‘overlayer’ nanojoints to graphene, indicating that the FEBID carbon ‘overlayers’ fully (i.e., with no connectivity breaks) link graphene and metal electrodes forming an electric interconnect.

To demonstrate the effect of FEBID carbon ‘overlayer’ nanojoints on electrical performance of the ML graphene device, two-terminal (drain-to-source) electrical measurements are adequate since gate voltage has no effect on electrical conductivity of the device in the case of multilayer graphene. The $I_{ds} - V_{ds}$ data in Fig. 8a show linear behavior indicating Ohmic contact at the ML graphene-FEBID carbon–Au junctions. Figure 8b shows the reduction of the device resistance with FEBID ‘overlayer’ nanojoints and inset shows the electrical measurement setup. Initial reduction of the device resistance by 14 % resulted from forming an additional conductive path for electrons through the FEBID of hydrogenated amorphous carbon (H:aC). Further reduction was achieved by post-deposition thermal annealing of FEBID nanojoints in vacuum ($P \sim 10^{-5}$ Torr)

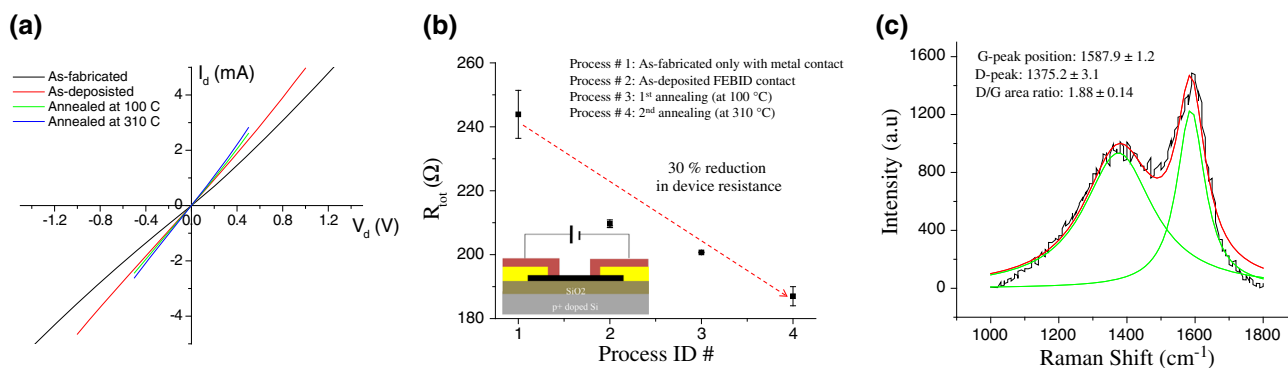


Fig. 8 **a** Electrical measurements for the ML graphene device with FEBID carbon ‘overlayer’ using the two-terminal method, **b** the reduction of the device electrical resistance achieved with FEBID

graphitic ‘overlayer’ nanojoints, and **c** Raman spectrum after thermal annealing at 310 °C in vacuum ($P \sim 10^{-5}$ Torr) indicating the graphitic structure of FEBID ‘overlayer’ nanojoints

resulting in graphitization and improvement of carbon electrical conductivity. The first annealing step was done at 100 °C (with the temperature ramp rate: 5 °C/min) during which the dehydrogenation occurs in the as-deposited FEBID H:c nanojoints [39], which led to reduction of the device resistance by only 4 %. After annealing at 310 °C, an additional decrease of the device resistance by 7 % was observed. The Raman G-band peak position and D/G area ratio for the annealed nanojoints were measured as $1,587.9 \text{ cm}^{-1}$ and 1.88 (Fig. 8c), respectively, indicating the partially graphitic structure with an increase of sp^2 carbon network domains. Overall, this multi-step procedure resulted in 30 % reduction of the device resistance with addition of FEBID graphitic conductive path, compared to the as-fabricated standard metal contact. One would expect that additional annealing at an elevated temperature or increasing the annealing time should further improve the contact resistance. Also, it is worth to note that further reduction of the contact resistance can be achieved by increasing contact width of FEBID nanojoints at ML graphene-metal interface.

The electrical properties of the graphene-metal contact are determined by the nature of electronic interactions, which are defined by molecular binding at the interface (i.e., physical/van der Waals vs. chemical/covalent bonding). Our DFT calculations shown in Fig. 1 indicate that the carbon atom as an interfacial link has strong chemical binding on the basal plane of graphene, and its binding energy is stronger than that of Ti contact to graphene, which is the best metallic material with contact resistivity of $2\text{e-}4 \text{ }\Omega\text{-m}$ [17, 20]. This suggests that FEBID graphitic nanojoints should also improve intrinsic interfacial property at the graphene-metal contact. Guided by this insight, device structures II and III were explored to improve the intrinsic interfacial property of graphene-metal contact using thin FEBID carbon ‘interlayers’.

Figure 9a shows the fabrication protocol of a ML graphene-metal interconnect with ‘post-deposited’ FEBID interlayer (Device structure II). An AFM image shows formation of the FEBID carbon interface to ML graphene with thickness of $\sim 7 \text{ nm}$, corresponding to ~ 21 layers of graphene. At the targeted graphene regions (red box), metal electrodes were fabricated using e-beam lithography followed by Au(20 nm)/Cr(10 nm) deposition and lift-off procedure. After fabrication of metal electrodes, focused electron beam with spot size 3 ($\sim 30 \text{ pA}$) and beam energy of 25 keV was exposed on top of ML graphene-metal contact areas to fabricate atomically thin FEBID carbon ‘interlayer’ using entrapped hydrocarbon contaminations as precursor molecules.

Device structure III described in Fig. 9b was fabricated by firstly depositing a thin FEBID carbon interlayer (thickness $\sim 1.4 \text{ nm}$) on ML graphene (thickness $\sim 3 \text{ nm}$) followed by Au (20 nm)/Cr (10 nm) deposition on top of FEBID carbon interlayer. While a complete, uniform surface coverage with FEBID carbon interlayer can be guaranteed in this device structure, interfacial coupling between the FEBID carbon interlayer and a metal electrode would be worse than that for a ‘post-deposited’ FEBID interlayer in the device structure II since metal deposition on ‘pre-deposited’ FEBID interlayer would result in a weak (physical interaction) binding similar to the standard metal contact to graphene. In order to enhance the interfacial property between FEBID carbon interlayer and metal, we additionally scanned the top of metal-FEBID interlayer-ML graphene contact areas by the focused electron beam, attempting to improve interfacial binding similar to the device structure II with the ‘post-deposited’ interlayer. For each ML graphene sample, reference standard metal contacts were also fabricated for side-by-side comparison of electrical performance. For all devices, thermal annealing in vacuum was performed to graphitize the FEBID carbon interlayers and to improve their electrical conductivity.

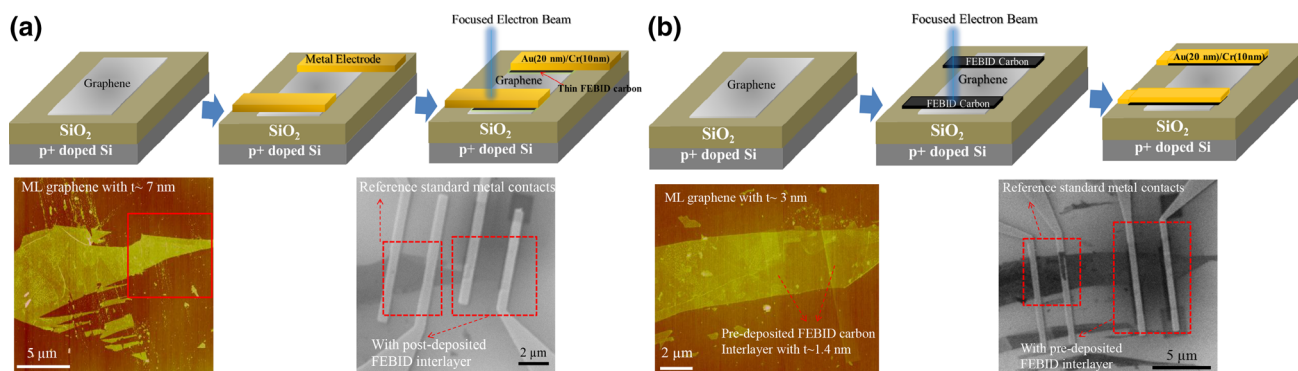


Fig. 9 Schematics and the corresponding AFM and SEM images for mechanically exfoliated ML graphene devices with (a) post-deposited (i.e., after pad metalization) and (b) pre-deposited (i.e., before pad

metalization) FEBID carbon ‘interlayer’ to improve intrinsic interfacial properties at the ML graphene-metal contacts

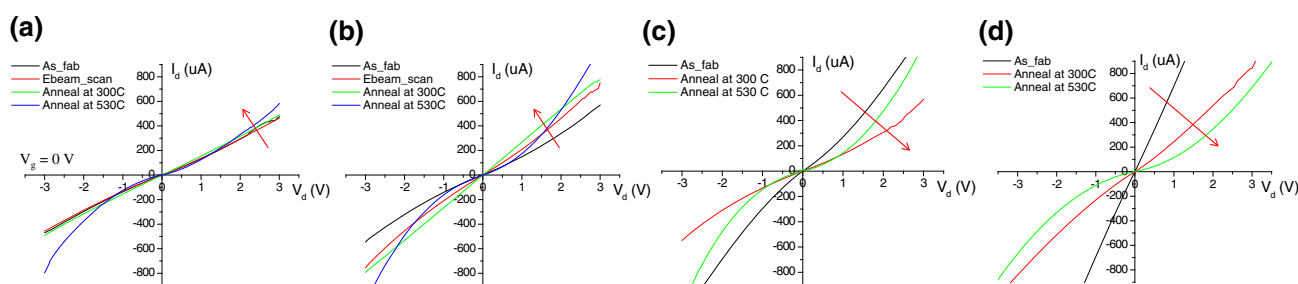


Fig. 10 Electrical measurements for devices with a post-deposited FEBID carbon ‘interlayer’, b pre-deposited FEBID carbon ‘interlayer’, c, d standard metal contacts only. All measurements were

performed at $V_g = 0$ V using two-terminal method, and thermal annealing was performed in vacuum, $P \sim 10^{-5}$ Torr

Figure 10 shows the $I_{ds} - V_{ds}$ measurements for all devices at zero back-gate voltage. Figure 10a, b is for the devices with post-deposited and pre-deposited FEBID carbon interlayer, respectively, while Fig. 10c, d is for the devices with a standard metal contact only for comparison. Focused electron beam scanning over the metal contact area, hereafter referred to as ‘post-deposition’ of FEBID interlayer, improved the electrical conductivity of a device with the pre-deposited FEBID interlayer (Fig. 10b), while it does not appear to make any significant contribution to the device with the post-deposited FEBID interlayer (Fig. 10a). It is clear that ‘post-deposition’ of FEBID carbon interlayer improves the interfacial property, but differences in contribution of the FEBID carbon interlayer in the two device structures are due to the parasitic deposition of a thin carbon film on the graphene conduction channel, which introduces scattering sites for electron transport. For the device with pre-deposited interlayer, graphene channel is already contaminated by a thin film of FEBID carbon during the pre-deposition and thus further contamination does not influence the electron transport through the graphene channel. However, for the device with post-deposited interlayer, the parasitic thin carbon film on top of ‘clean’ graphene channel increases the channel resistance of the as-fabricated device, along with improving the

intrinsic interfacial binding and electronic coupling at the graphene-metal contact. Thus, one can expect that there should be a ‘trade-off’ between an increase of the channel resistance due to the parasitic deposition of carbon versus the reduction of the contact resistance owing to the improved electronic coupling at the contact interface. Interestingly, despite a negative effect of FEBID carbon on the channel resistance, one finds that the devices with the FEBID interlayers exhibit an improved electrical conductivity upon thermal annealing in vacuum. On the other hand, annealing of standard metal contacts does degrade performance (Fig. 10c, d), likely due to interfacial breakdown.

In order to clearly identify the contribution of the graphitic interlayer, the linearity of $I_{ds} - V_{ds}$ curves (an indicator of Ohmic contact) and device resistance normalized by the contact width (yielding the device resistivity) are examined in Fig. 11a, b, respectively. Focused electron beam scanning (process ID #2) and thermal annealing at a moderate temperature (310 °C) in vacuum (process ID #3) improved the I–V linearity (Ohmic behavior) almost to an ideal limit with a FEBID interlayer, while thermal annealing of devices with standard metal contacts (Fig. 11a) even at low temperature degraded the linearity of I–V curves. The same trend can

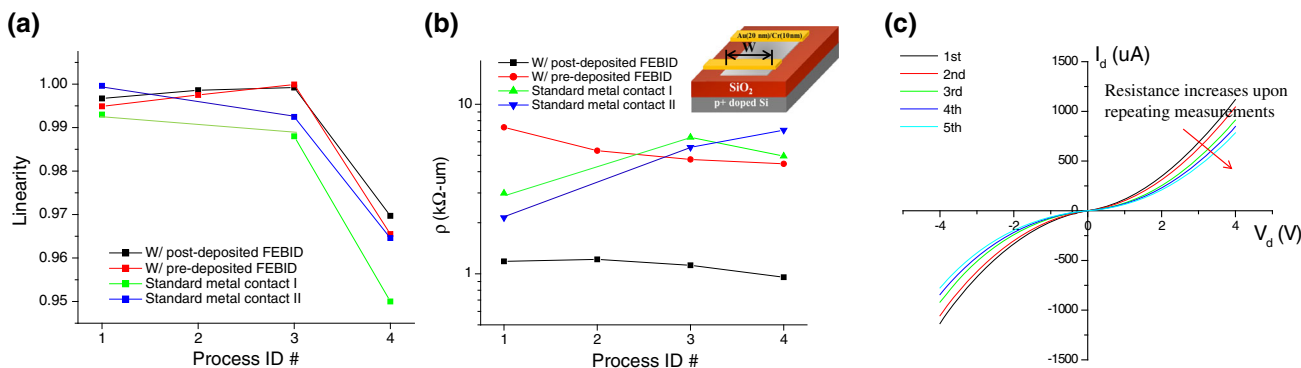


Fig. 11 **a** Linearity of $I_{ds} - V_{ds}$ curves after each step (process ID) of the experimental process, and **b** device resistivity (normalized by contact width) for graphene devices with post- and pre-deposited FEBID carbon interlayer versus reference devices with only standard metal contacts. **c** Repeated measurements after high temperature

annealing at 530 °C by sweeping the bias from -4 to 4 V, resulting in an increase of the device resistance which indicates the interfacial breakdown. Process ID #1: as-fabricated, #2: focused electron beam scanning over graphene-metal contact area, #3: annealed at 300 °C, and #4: annealed at 530 °C

be observed in the device resistivity in Fig. 11b. This result implies that FEBID interlayer improves both the electrical and thermo-mechanical properties at the graphene and metal interfaces. However, after high temperature annealing (530 °C), the linearity for all devices decreased showing the rectifying behavior, and the device resistance continues to increase after repeating the bias voltage sweep from -4 to 4 V as shown in Fig. 11c, which indicates that the interfaces are degraded when excessive temperature is applied for interface conditioning. Device resistivity after high temperature annealing (process ID #4) in Fig. 11b was obtained from the initial measurement of $I_{ds} - V_{ds}$ before degradation due to repeated electrical biasing. While repeating the bias voltage sweep increases the electrical resistivity of all devices, high temperature annealing (process ID #4) reduces the device resistivity with FEBID interlayer, as shown in Fig. 11b. It is likely owing to an increased graphitization (and improved electrical conductivity) of the interlayer despite the interfacial breakdown. Yet, after repeated measurements, the interfacial breakdown appears to overwhelm the improvement of the interface electrical conductivity due to the FEBID graphitic interlayer, which poses a significant challenge to practical applications of the proposed interface improvement method. These observations motivate additional efforts to understand the mechanism of interface degradation upon annealing and to develop an improved methodology for graphitizing the FEBID carbon “interlayer” interface at low temperature.

2.4.3 FEBIE for resist-free patterning of graphene devices

A high-resolution and resist-free graphene patterning technique is one of key enabling technologies directly relevant to fabrication of graphene devices. The electronic

state of graphene can be tuned by controlling its width and edge structure. For example, interconnect applications require graphene with metallic characteristics, whereas transistors require graphene to be semiconducting with a definite band gap. To this end, we and other groups explored the reactive gas-assisted focused-electron-beam-induced etching (FEBIE) of graphene [36–38]. An in-house-developed gas injection system was used to introduce the focused O₂ flow onto designated areas of graphene for etching, as shown in Fig. 12. Ionization of O₂ gas molecules by electron beam exposure results in the highly reactive ionized O₂ gas plasma, which reacts with/oxidizes carbon atom of graphene. Figure 12 compares the AFM images of the areas exposed and unexposed to EBIE. It shows that FEBIE results in formation of the porous structure in graphene with the nanopits of the depth around 6 nm. Using a similar approach, Thiele and co-workers demonstrated “direct-write” graphene patterning via FEBIE with spatial resolution better than 20 nm [38]. This initial demonstration of possibility to etch graphene using electron beam is a promising result, and with further fundamental understanding and optimization, FEBIE has a potential to become a powerful technique for resist-free patterning of graphene.

2.4.4 Energetic inert gas jet for control of conduction channel contamination in FEBID

Parasitic deposition of a carbon “halo” film due to both the widely spread, high-energy backscattered primary electrons and longer range secondary electrons reaching the graphene surface outside of the metal-graphene contact area has a detrimental effect on the electronic properties of the pristine conduction channel due to high sensitivity of graphene to doping by adsorbed or surface-bound impurities. Thus, if FEBID were to be successfully used for

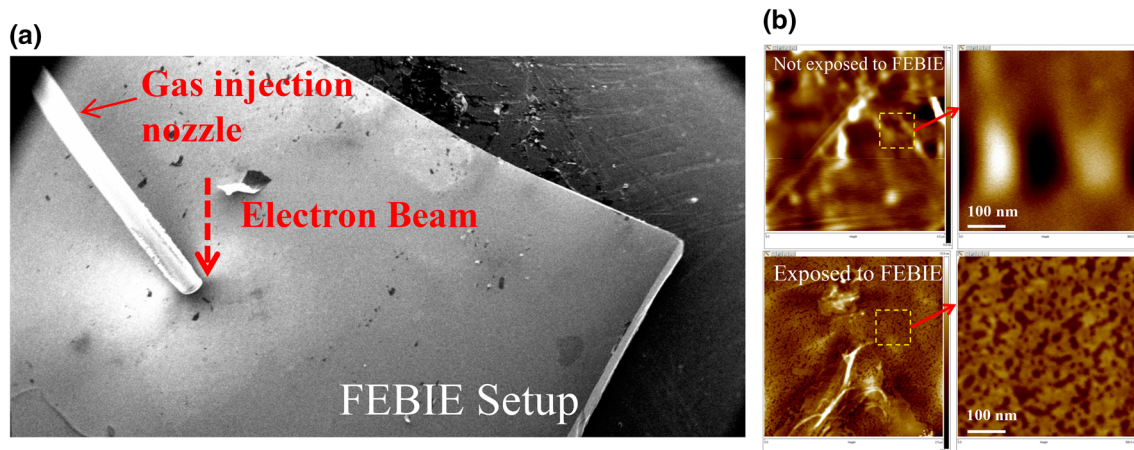


Fig. 12 **a** SEM image showing the gas injection system for FEBIE (electron-beam-induced etching) procedure, and **b** AFM images of the graphene surfaces exposed and unexposed to FEBIE, which shows the

FEBIE produces uniformly distributed, etched nanopits (depth ~ 6.5 nm) on the graphene surface

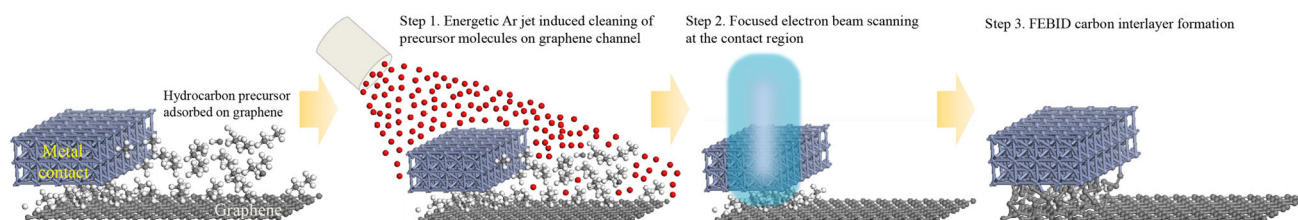


Fig. 13 Schematic of the FEBID carbon “interlayer” fabrication procedure as a contact between metal and graphene with an assistance of energetic, inert (e.g., Ar) gas jet for cleaning of precursor molecules from the graphene conduction channel

making contacts to graphene-based electronic devices a provision needs to be made for managing this parasitic carbon film deposition. One promising approach to this challenge is to exploit the impact-induced desorption of the surface-bound contaminants, including hydrocarbon species acting as precursors for FEBID, by impingement of high kinetic energy jet of inert gas molecules prior to turning the electron beam on for deposition [32]. This is the third and important “leg” of the multi-functional FEBIP environment [33], which we advocate in this article as the way forward for the FEBIP application as a “direct-write” multi-functional tool for carbon nanoelectronics. Importantly, such an energetic gas jet can be readily integrated within the SEM chamber of a typical FEBIP setup (see, for example, Fig. 12), thus minimizing the number of auxiliary steps prone for picking up additional contamination between the surface cleaning and deposition/etching processes in a typical device fabrication workflow. We have shown that an energetic inert (Ar) gas jet is as an effective means to enhance desorption of hydrocarbon contaminants from the substrate for the surface cleaning during SEM imaging, which minimizes the parasitic carbon deposition [32]. Figure 13 shows one of possible workflows for energetic-gas-jet-assisted FEBIP of metal-to-graphene interconnect, which utilizes this

technique to remove the adsorbed contaminants/possible precursors from the graphene conduction channel regions, while selectively depositing FEBID carbon interlayer only at the graphene-metal contact region where precursor source remains protected under the metal.

2.5 FEBIP+ X methods for resist-free semiconductor nanostructure manufacturing

In this section, we briefly highlight an emergence of hybrid techniques, which exploit unique capabilities of FEBIP for high-resolution, negative (deposition)/positive (etching) resist-free patterning in combination with batch material deposition/removal chemistry, for solving some of the key challenges of semiconductor manufacturing industry. While the standard semiconductor fabrication techniques, such as plasma etching, ion etching, and deep reactive ion etching (DRIE), have successfully been used to fabricate electronic devices of varying degrees of complexity, two issues remain unresolved as feature sizes shrink into the nanoscale. First, fabrication of high-aspect-ratio nanostructures with smooth side walls has been elusive. For example, the maximum aspect ratio of silicon nanowires achievable with DRIE fabrication can be pushed to about $\sim 50:1$; however, the process leaves very rough and

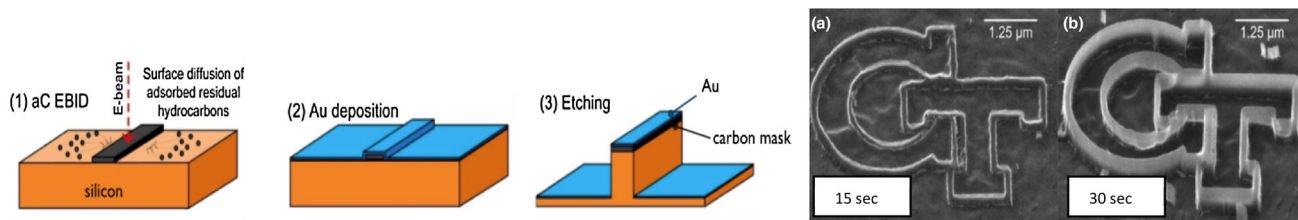
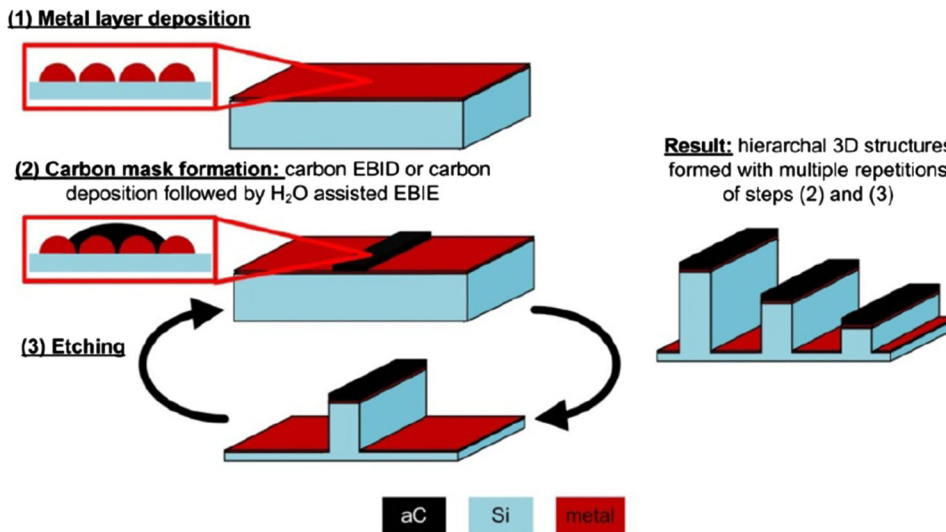


Fig. 14 Schematic of a three-step process “direct-write” process with (1) FEBID carbon “hard” masking, (2) metal (gold) catalyst deposition, and (3) area selection MaCE silicon removal, yielding in high-aspect-ratio-free standing silicon nanostructures of complex

geometry and straight walls, shown in progression of SEM images of Georgia Tech logo with 100 nm line-width etched for **a** 15 s, resulting in ~225 nm wall height and **b** 30 s, resulting in ~700 nm wall height

Fig. 15 Process flow diagram for hybrid FEBID/FEBIE-MaCE resulting in hierarchal 3D nanostructure fabrication



scalloped sidewalls. Second, and perhaps most critical, the need for resist layer spinning limits application of resist-based masking techniques in making complex nanostructures with varying feature height in subsequent fabrication steps. A hybrid (FEBIP+X) approach, which combines the focused-electron-beam-assisted deposition/etching (FEBID/FEBIE) of amorphous carbon (aC) with metal-assisted chemical etching (MaCE) has a unique features that could help address both of these challenges.

The FEBIP+MaCE method exploits a well-established chemistry of substrate-selective MaCE in novel combination with carbon deposition by FEBID as a “negative” masking step and/or carbon removal by water/oxygen-assisted FEBIE as a “positive” masking step to make unique three-dimensional nanostructures on semiconductor substrates. The speed of FEBID carbon mask deposition is comparable to the writing speed of Electron Beam Lithography, while the MaCE etching rate is known to be in the range of etching rates of DRIE. We have established an essential proof of principle for the proposed FEBID/FEBIE-MaCE process—that is that the 3–4-nm-thick barrier layer of amorphous carbon (aC) can be imbedded using FEBID underneath the layer of metal catalyst nanoparticles to locally block MaCE of silicon substrate with nanoscale

resolution (sub 10 nm), thus yielding a “negative” mask for complex nanostructure fabrication (Fig. 14). With optimized process parameters, such as catalyst nanoparticle size distribution and FEBID masking procedure, fabrication of solid 3D silicon nanostructures with sharp edges and straight walls has been demonstrated [53, 54].

To achieve a capability for hierarchical fabrication of different aspect ratio nanostructures on the same semiconductor substrate (e.g., Fig. 15), the fabrication steps need to be interchanged by first depositing the metal nanoparticle catalyst layer everywhere on the substrate surface and then using either FEBID or FEBIE to create “negative” or “positive” carbon masks atop of the metal layer followed by a timed MaCE etching after each masking step. Thus, FEBID of carbon on top of densely packed metal particles, which is required for MaCE of 3D structures, will also yield a thin carbon layer beneath and in-between the particles. Similarly, water/oxygen-assisted FEBIE can locally remove an evaporated/sputtered carbon film from the top and within the interparticle spaces of the porous metal catalyst network. Since the metal nanoparticles always remain in direct contact with a semiconductor substrate, each MaCE step can be followed by FEBID/FEBIE of another carbon mask, resulting in fabrication of hierarchal nanostructures of

varied height and topological complexity. Upon multiple masking-etching steps, including a possibility for substrate tilting and rotation during FEBID/FEBIE masking steps, essentially an arbitrarily topologically complex 3D semiconductor nanostructure or an array of nanostructures will emerge. Such high-aspect-ratio hierarchical nanostructures with complex 3D geometry [55] should enable a much greater functionality, which are beyond the capabilities of conventional lithographic + batch deposition/etch chemistry approaches used for semiconductor manufacturing and will, without doubt, be beneficial to a host of existing and new applications of opto-electro-mechanical devices and new integrated circuit architectures.

3 Summary and outlook

Focused-electron-beam-induced processing (FEBIP) is an emerging method for “direct-write” fabrication of topologically complex three-dimensional nanostructures from a variety of materials, which is relatively low cost, inflicts minimal surface damage to the substrate, and can achieve high feature resolution. Despite these compelling capabilities, until recently the FEBIP application to electronics manufacturing has been limited to specialized niches, such as for example lithographic mask repair. This is likely due to limited throughput of the technique and scalability challenges common to all beam-based manufacturing techniques which make parts sequentially, one at the time. However, an emergence of new electronic materials, such as carbon nanotubes and graphene, brings about both the new opportunities as well as unique challenges to their patterning and processing methods, especially in the case of hybrid devices which require integration of conventional CMOS with carbon components. In this context, the needs for circuit customization and managing electrical/thermal/mechanical interfaces associated with integration of dissimilar materials make the flexibility afforded by the FEBIP’s “direct-write” capability appealing. This is further amplified by a fact that electron-beam-induced deposition has some unique aspects that are fundamentally not possible to accomplish using any other conventional integrated circuit fabrication techniques. In particular, an ability to modify the buried interfaces, which are externally inaccessible, via the penetrating electrons of appropriately tuned beam energy, and to form the imbedded deposits performing as an interfacial “glue” with tunable electrical/thermal/mechanical properties (e.g., poorly conducting but highly compliant amorphous carbon vs. graphitic carbon with its superior electrical and thermal conductivity) provide intriguing opportunities to enable unique applications for carbon nanoelectronics.

The materials processing capabilities offered by FEBIP are especially compelling when it is done in combination with other “beams” of energetic particles (photon, molecules, etc.), as it establishes an intimately integrated multi-functional processing environment that has a potential for realizing the Richard Feynman’s vision for the focused beam-based additive nanomanufacturing—that is “we could write with that spot like we write in a TV cathode ray oscilloscope, by going across in lines, and having an adjustment which determines the amount of material which is going to be deposited as we scan in lines.” It is our opinion that this avenue for future FEBIP development is most promising from the applications’ prospective, as an emerging multi-functional (electron/photon/molecule beam) FEBID/FEBIE operation would enable one to define shapes (patterning), form structures (deposition/etching), and modify (cleaning/doping/annealing) properties with locally resolved control on nanoscale within the same tool without ever changing the processing environment. This, in turn, should allow for (1) increasing the process throughput by minimization of a number of intermediate “handling steps” (which is a deficiency for all beam-based techniques as compared to batch fabrication), (2) the possibility to create almost an arbitrarily diverse portfolio of different device structures/functionalities on the same substrate due to “direct-write” nature of the approach, and (3) the capability for local property control/modification while minimizing the parasitic substrate contamination in the course of processing, which is especially critical for graphene-like electronic materials, whose properties are highly sensitive to intended or unintended dopants.

While development and transition to industrial use of multi-functional FEBIP environment will require substantial advances in both fundamental understanding of multiple interacting processes and new technological solutions and, therefore, has longer term horizon, the hybrid approaches combining FEBIP with standard batch semiconductor processing methods have near to mid-term potential for impacting the practical applications by extending the range of possible structures and device architectures that can be produced using conventional techniques. An example of such a hybrid approach, the FEBID/FEBIE-MaCE process, is as fast in pattern definition and etching speed as any other nanostructure fabrication techniques, but, owing to its resist-free nature, it is significantly simpler, more flexible and robust as compared to the current state-of-the-art 3D nanofabrication techniques. Furthermore, the FEBID/FEBIE-MaCE process also has potential for controllable pattern definition of sub 10 nm features that enable formation of high-aspect-ratio 3D nanostructures with smooth walls. This yields a versatile and low-cost fabrication method (FEBID/FEBIE-MaCE) of high-aspect-ratio hierarchical 3D semiconductor

nanostructures with complex topology and through-depth-variable geometry.

Lastly, with recent advances in development of multi-electron-beam systems, there is an expectation that a diverse family of emerging FEBIP-based techniques, including those summarized in this article, can be further scaled up to achieve a substantial increase in throughput, which will further enhance its cost competitiveness and should promote greater penetration to a broad range of semiconductor device manufacturing and materials processing applications. This provides strong motivation for in-depth fundamental studies of interacting physical, chemical, and engineering aspects of this very potent “direct-write” nanomanufacturing technology, as well as active exploration of new FEBIP applications to emerging fields of carbon nanoelectronics and hybrid opto-electro-mechanical devices.

Acknowledgments This material is based on work supported by the Semiconductor Research Corporation under GRC Contract Nos. 2008-OJ-1864 and 2011-OJ-2221 (FEBIP of CNT and graphene interconnects), the Air Force Office of Scientific Research BIONIC Center under Award No. FA9550-09-1-0162 (FEBIP for graphene surface modification), the U.S. Department of Energy, Office of Basic Energy Sciences, Division of Materials Sciences and Engineering under Award No. DE-SC0010729 (energetic-gas-jet FEBIP) and the National Science Foundation under Award No. DMI-0403671 (FEBID-MaCE for hierarchical silicon nanostructures). CVD grown graphene samples used in this work were provided the Air Force Research Laboratory, Materials and Manufacturing Directorate (S. Kim, S. Paclay and A. Voevodin). Collaboration with K. Rykaczewski and O. Hildreth on FEBID-MaCE is appreciated. We also thank K. Rykaczewski for his early contributions and experimental assistance with FEBID of CNT interconnects. Insightful discussions and guidance by R. Caudillo (Intel) and A. Chen (Global Foundries) on electrical characterization of graphene-based electronic devices are appreciated.

References

1. A. Naeemi, R. Sarvari, J.D. Meindl, Performance comparison between carbon nanotube and copper interconnects for gigascale integration (GSI). *IEEE Electr. Dev. Lett.* **26**(2), 84–86 (2005)
2. W. Steinhögl, G. Schindler, G. Steinlesberger, M. Engelhardt, Size-dependent resistivity of metallic wires in the mesoscopic range. *Phys. Rev. B* **66**, 075414 (2002)
3. ITRS: International Technology Roadmap for Semiconductors (2011 ed). <http://www.itrs.net>
4. R.S. Ruoff, D.C. Lorents, Mechanical and thermal properties of carbon nanotubes. *Carbon* **33**, 925–930 (1995)
5. C. Lee, X. Wei, J. Kysar, J. Hone, Measurement of elastic properties and intrinsic strength of monolayer graphene. *Science* **321**, 385–388 (2008)
6. A.K. Geim, K.S. Novoselov, The rise of graphene. *Nat. Mater.* **6**, 183–191 (2007)
7. M.S. Dresselhaus, G. Dresselhaus, P. Avouris, *Carbon Nanotubes: Synthesis, Structure, Properties, and Applications* (Springer, Berlin, 2001)
8. A. Naeemi, J.D. Meindl, Compact physical models for multiwall carbon–nanotube interconnects. *IEEE Electr. Dev. Lett.* **27**, 338–340 (2006)

9. A.D. Franklin, Z. Chen, Length scaling of carbon nanotube transistors. *Nat. Nanotechnol.* **5**, 858–862 (2010)
10. R.V. Seidel, A.P. Graha, J. Kretz, B. Rajasekharan, G.S. Duesberg, M. Liebau, E. Unger, F. Kreupl, W. Hoenlein, Sub-20 nm short channel carbon nanotube transistors. *Nano Lett.* **5**(1), 147–150 (2005)
11. S. Frank, P. Poncharal, Z.L. Wang, W.A. de Herr, Carbon nanotube quantum resistors. *Science* **280**(5370), 1744–1746 (1998)
12. H.J. Li, W.G. Lu, J.J. Li, X.D. Bai, C.Z. Gu, Multichannel ballistic transport in multiwall carbon nanotubes. *Phys. Rev. Lett.* **95**(8), 086601 (2005)
13. R. Pati, Y. Zhang, S.K. Nayak, P.M. Ajayan, Effect of H₂O adsorption on electron transport in carbon nanotube. *Appl. Phys. Lett.* **81**(14), 2638–2640 (2002)
14. J. Tersoff, Contact resistance of carbon nanotubes. *Appl. Phys. Lett.* **74**(15), 2122–2124 (1999)
15. J.J. Palacios, A.J. Perez-Jimenez, E. SanFabian, J.A. Verges, First-principles phase-coherent transport in metallic nanotubes with realistic contacts. *Phys. Rev. Lett.* **90**(10), 106801 (2002)
16. M.S. Wang, D. Golberg, Y. Bando, Superstrong low-resistant carbon nanotube-carbide-metal nanocontacts. *Adv. Mater.* **22**(47), 5350–5355 (2010)
17. A.D. Franklin, S.-J. Han, A.A. Bol, W. Haensch, Effects of nanoscale contacts to graphene. *IEEE Electron. Dev. Lett.* **32**(8), 1035–1037 (2011)
18. A.D. Franklin, S.-J. Han, A.A. Bol, V. Pereveinos, Double contacts for improved performance of graphene transistors. *IEEE Electron Device Lett.* **33**(1), 17–19 (2012)
19. Y. Matsuda, W.Q. Deng, W.A. Goddard, Contact resistance properties between nanotubes and various metals from quantum mechanics. *J. Phys. Chem. C* **111**, 11113–11116 (2007)
20. Y. Matsuda, W.Q. Deng, W.A. Goddard, Contact resistance for “end-contacted” metal-graphene and metal-nanotube interfaces from quantum mechanics. *J. Phys. Chem. C* **114**, 17845–17850 (2010)
21. J. Smith, A.D. Franklin, D.B. Farmer, C.D. Dimitrakopoulos, Reducing contact resistance in graphene devices through contact area patterning. *ACS Nano* **7**(4), 3661–3667 (2013)
22. S.J. Randolph, J.D. Fowlkes, P.D. Rack, Focused, nanoscale electron-beam-induced deposition and etching. *Crit. Rev. Sol. State Mater. Sci.* **31**(3), 55–89 (2006)
23. N. Silvis-Cividjian, C.W. Hagen, P. Kruit, Spatial resolution limits in electron-beam-induced-deposition. *J. Appl. Phys.* **98**, 084905–084912 (2005)
24. W.F. van Dorp, C.W. Hagen, P.A. Crozier, P. Kruit, Growth behavior near the ultimate resolution of nanometer scale focused electron beam-induced deposition. *Nanotechnology* **19**(22), 225305 (2008)
25. J.C. Meyer, C.O. Girit, M.F. Crommie, A. Zettl, Hydrocarbon lithography on graphene membranes. *Appl. Phys. Lett.* **92**, 123110 (2008)
26. K. Rykaczewski, M.R. Henry, S.K. Kim, A.G. Fedorov, D. Kulkarni, S. Singamaneni, V.V. Tsukruk, The effect of the geometry and material properties of a carbon joint produced by electron beam induced deposition on electrical resistance of a multiwalled carbon nanotube-to-metal contact interface. *Nanotechnology* **21**(3), 0352021–03520212 (2010)
27. L. Mandeltort, P. Choudhury, J.K. Johnson, J.T. Yates, Methyl radical reactivity on the basal plane of graphite. *J. Phys. Chem. C* **116**, 18347–18357 (2012)
28. A.V. Krashennikov, K. Nordlund, P.O. Lehtinen, A.S. Foster, A. Ayuela, R.M. Nieminen, Adsorption and migration of carbon adatoms on carbon nanotubes: Density-functional ab initio and tight-binding studies. *Phys. Rev. B.* **69**, 073402 (2004)
29. K. Rykaczewski, W.B. White, A.G. Fedorov, Analysis of electron beam induced deposition (EBID) of residual hydrocarbons in

- electron microscopy. *J. Appl. Phys.* **101**(5), 054307–054319 (2007)
30. K. Rykaczewski, A. Marshall, W.B. White, A.G. Fedorov, Dynamic growth of carbon nanopillars and microrings in electron beam induced dissociation of residual hydrocarbons. *Ultramicroscopy* **108**(9), 989–992 (2008)
 31. T.H.P. Chang, M. Mankos, K.Y. Lee, L.P. Muray, Multiple electron-beam lithography. *Microelectron. Eng.* **57–58**, 117–135 (2001)
 32. M.R. Henry, S.K. Kim, K. Rykaczewski, A.G. Fedorov, Inert gas jets for growth control in electron beam induced deposition. *Appl. Phys. Lett.* **98**(26), 263109 (2011)
 33. I. Utke, P. Hoffmann, J. Melngailis, Gas-assisted focused electron beam and ion beam processing and fabrication. *J. Vac. Sci. Technol. B* **26**(4), 1197–1276 (2008)
 34. R. Winkler, J. Fowlkes, A. Szkudlarek, I. Utke, P.D. Rack, H. Plank, The nanoscale implications of a molecular gas beam during electron beam induced deposition. *ACS Appl. Mat. Interfaces*. doi:10.1021/am405591d. (2014)
 35. S.K. Kim, D.D. Kulkarni, K. Rykaczewski, M. Henry, V.V. Tsukruk, A.G. Fedorov, Fabrication of an ultra-low-resistance, ohmic contact to MWCNT-metal interconnect using graphitic carbon by electron beam induced deposition (EBID). *IEEE Trans. Nanotechnol.* **11**(6), 1223–1230 (2012)
 36. S.K. Kim, D.D. Kulkarni, S. Jang, M. Henry, V.V. Tsukruk, A.G. Fedorov, Graphitic FEBID carbon interfaces between MWCNT/graphene and metal electrodes. Poster presentation, *Materials Research Society Spring 2013 Meeting* (San Francisco, CA, April 1–5, 2013)
 37. D. Fox, A. O'Neill, D. Zhou, M. Boese, J.N. Coleman, H.Z. Zhang, Nitrogen assisted etching of graphene layers in a scanning electron microscope. *Appl. Phys. Lett.* **98**, 243117 (2011)
 38. C. Thiele, A. Felten, T.J. Echtermeyer, A.C. Ferrari, C. Casiraghi, H.V. Lohneysen, R. Krupke, Electron-beam-induced direct etching of graphene. *Carbon* **64**, 84–91 (2013)
 39. D.D. Kulkarni, K. Rykaczewski, S. Singamaneni, S. Kim, A.G. Fedorov, V.V. Tsukruk, Thermally induced transformation of amorphous carbon nanostructures fabricated by electron beam induced deposition. *ACS Appl. Mater. Interfaces* **3**(3), 710–720 (2011)
 40. D. Kulkarni, S.-K. Kim, A.G. Fedorov, V.V. Tsukruk, Fast light-induced phase transformations of carbon on metal nanoparticles. *Adv. Funct. Mat.*, **22**(10), 2129–2139 (2012)
 41. N.A. Roberts, J.D. Fowlkes, G.A. Magel, P.D. Rack, Enhanced purity and resolution via laser assisted electron beam induced deposition of platinum. *Nanoscale* **5**(1), 408–415 (2013)
 42. F. Xia, V. Perebeinos, Y. Lin, Y. Wu, P. Avouris, The origins and limits of metal-graphene junction resistance. *Nat. Nanotechnol.* **6**, 179–184 (2011)
 43. Y. Chai, A. Hazeghi, K. Takei, H.Y. Chen, P.C.H. Chan, A. Javey, H.S.P. Wong, Low-resistance electrical contact to carbon nanotubes with graphitic interfacial layer. *IEEE Trans. Electron Device* **59**(1), 12–19 (2012)
 44. S.C. Lim, J.H. Jang, D.J. Bae, G.H. Han, S. Lee, I.S. Yeo, Y.H. Lee, Contact resistance between metal and carbon nanotube interconnects: effect of work function and wettability. *Appl. Phys. Lett.* **95**(26), 264103 (2009)
 45. M. Shiraishi, M. Ata, Work function of carbon nanotubes. *Carbon* **39**(12), 1913–1917 (2001)
 46. C.H. Jin, J.Y. Wang, Q. Chen, L.M. Peng, In situ fabrication and graphitization of amorphous carbon nanowires and their electrical properties. *J. Phys. Chem. B* **110**, 5423–5428 (2006)
 47. A. Callegari, D.A. Buchanan, H. Hovel, E. Simonyi, A. Marwick, Thermal stability and electrical properties of hydrogenated amorphous carbon film. *Appl. Phys. Lett.* **65**(25), 3200–3202 (1994)
 48. K. Rykaczewski, M. Henry, A.G. Fedorov, Electron beam induced deposition of residual hydrocarbons in the presence of a multiwall carbon nanotube. *Appl. Phys. Lett.* **95**(11), 113112–113115 (2009)
 49. A.G. Fedorov, K. Rykaczewski, *Electron Beam Induced Deposition of Interface to Carbon Nanotube*. U.S. Patent No. 8,207,058 (2012)
 50. A.C. Ferrari, J. Robertson, Interpretation of raman spectra of disordered and amorphous carbon. *Phys. Rev. B* **61**, 14095–14107 (2000)
 51. Y. Sui, J. Appenzeller, Screening and interlayer coupling in multilayer graphene field-effect transistors. *Nano Lett.* **9**(8), 2973–2977 (2009)
 52. S.M. Song, J.K. Park, O.J. Sul, B.J. Cho, Determination of work function of graphene under a metal electrode and its role in contact resistance. *Nano Lett.* **12**, 3887–3892 (2012)
 53. K. Rykaczewski, O.J. Hildreth, D. Kulkarni, M. Henry, S.-K. Kim, C.P. Wong, V.V. Tsukruk, A.G. Fedorov, Maskless and resist-free rapid prototyping of three dimensional silicon structures through Electron Beam Induced Deposition (EBID) of carbon in combination with Metal assisted Chemical Etching (MaCE) of Silicon. *ACS Appl. Mat. Interfaces* **2**(4), 969–973 (2010)
 54. K. Rykaczewski, O.J. Hildreth, C.P. Wong, A.G. Fedorov, J.H.J. Scott, Directed 2D-to-3D pattern transfer method for controlled fabrication of topologically complex three-dimensional features in silicon. *Adv. Mater.* **23**(5), 659–663 (2011)
 55. K. Rykaczewski, O.J. Hildreth, C.P. Wong, A.G. Fedorov, J.H.J. Scott, Guided three-dimensional catalyst folding during metal-assisted chemical etching of silicon. *Nano Lett.* **11**(6), 2369–2374 (2011)

Copyright of Applied Physics A: Materials Science & Processing is the property of Springer Science & Business Media B.V. and its content may not be copied or emailed to multiple sites or posted to a listserv without the copyright holder's express written permission. However, users may print, download, or email articles for individual use.